



1 Variability of Relativistic Electron Flux ($E > 2$ MeV) during Geo-Magnetically 2 Quiet and Disturbed days: A Case Study

3

4 **Tulsi Thapa^{1,2}, Binod Adhikari^{1,3}, Prashrit Baruwal⁴, Kiran Pudasainee¹**

5 ¹Department of Physics, St. Xavier's College, Maitighar, Kathmandu, Nepal

6 ²National Astronomical Observatories of China, University of Chinese Academy of Sciences,
7 China

8 ³Department of Physics, Patan Multiple Campus, Tribhuvan University, Kathmandu, Nepal

9 ⁴Central Department of Physics, University Campus, Tribhuvan University, Kirtipur, Nepal

10 **Corresponding Author: *binod.adhi@gmail.com***

11 Abstract

12 We analyzed the relativistic electron fluxes ($E > 2$ MeV) during three different geomagnetic
13 storms: moderate, intense, and super-intense and one geo-magnetically quiet period. We have
14 opted Continuous wavelet analysis and cross-correlation technique to extend current
15 understanding and of the radiation-belt dynamics. We found that the fluctuation of relativistic
16 electron fluxes dependent basically on prolonged southward interplanetary magnetic field IMF-
17 Bz. Cross-correlation analysis depicted that SYM-H does not show a strong connection either
18 with relativistic electron enhancement events or persistent depletion events. Our result supports
19 the fact that geomagnetic storms are not a primary factor that pumps up the radiation belt. In fact
20 they seem event specific; either depletion or enhancement or slight effect on the outer radiation
21 belt might be observed depending on the event. Solar wind pressure and velocity were found to
22 be highly and positively correlated with relativistic electron. We found that, the count of
23 relativistic electron flux (> 2 MeV) decreases during the main phase of geomagnetic storm with
24 the increase in -- from quiet to super intense storm -- geomagnetic storm conditions (Table 1).
25 However, Psw was found to be weakly correlated in case of intense storms following an abrupt
26 increase of electron flux for ~4 hrs, which is interesting and unique.

27

28 **Keywords:** Geomagnetic Storms, Relativistic Electron, Cross-Correlation, Continuous Wavelet
29 Transform



30 1. Introduction

31 The major plasma sources in the interplanetary medium responsible for geomagnetic
32 disturbances are identified as coronal mass ejection (CMEs), which include the magnetic cloud,
33 interplanetary shock, the co-rotating interaction region (CIR) and the high-speed solar wind
34 streamers[Gosling et al., 1991]. The interaction between those interplanetary structures with the
35 Earth's magnetosphere-ionosphere system can produce effects such as geomagnetic storms, sub
36 storms and trapping of high energy charge particles in the radiation belt, known as Van Allen
37 belt[Mauk et al., 2012]. There are various solar wind parameters that are effective enough to
38 fluctuate the content of relativistic electron flux. Enhancement in relativistic electron fluxes might
39 be an important sources of energy input and chemical change to the middle atmosphere.
40 Magnetic reconnection is the main physical phenomena transporting energy from the solar wind
41 into the magnetosphere.

42

43 Van Allen radiation belts are composed of ions, protons and electrons with energy ranging from
44 100 keV to 10 MeV. It consists of two belts: inner and outer radiation belt. Outer radiation belt
45 usually lies at an altitude of 3 Earth radii (R_E) and extending to 10 R_E above the Earth's surface
46 where GPS satellites, metrological satellites, broadcasting and communication satellites are
47 operating [R. Kataoka and Y. Miyoshi, 2008]. The increasing dependency on modern
48 infrastructure and technology and expanding human presence in space drags us more for the
49 comprehensive study and understanding of space weather and their dynamics [Baker et al.,
50 2000]. For the deeper understanding of the structure and dynamics of Earth's radiation belt,
51 NASA developed the Van Allen Probes mission [Mauk et al., 2012]. The aftermath of highly
52 fluctuating electron fluxes in the Earth's outer radiation belt might be its acceleration and loss.
53 Paulikas & Blake [1979] reported such rapid acceleration and loss of relativistic electrons.
54 Reeves et al., [2003] and Turner et al. [2013] added relativistic electron population in the
55 radiation belt can not only subsidize but also can be enhanced, depleted, or even not affected at
56 all due to the acceleration and loss mechanism. Pinto et al. [2018] identified and analyzed 61
57 relativistic electron enhancement events and 21 depletion events during 1996 to 2006, resulting
58 the persistent depletion events are characterized by: a low V_{sw} , a sudden increase in proton
59 density, and a northward turning of IMF Bz. Also, predicted their threshold values.

60



61 This work focuses on the loss, acceleration, and transport of relativistic electron $E >$
62 2 MeV during three different geomagnetic storms: moderate, intense, and super-intense and one
63 geo-magnetically quiet period.

64

2. Dataset and Methodologies

65 The datasets has been extracted from OMNI (Operating Mission as Nodes on the Internet)
66 webpage and downloaded from the official website of NASA
67 <https://omniweb.gsfc.nasa.gov/dataset> to study solar wind parameters. The integrated fluxes of
68 electrons with energies $E > 2\text{ MeV}$ at geosynchronous orbit ($L = 6.6$) for our study are collected
69 from the GOES-8 and GOES-12; *Geostationary Operational Environment Satellites*
70 (*GOES*; <http://www.ngdc.noaa.gov/stp/satellite/goes/dataaccess.html>). This database provides 1
71 min temporal resolution data obtained from the sets of ACE, Wind, and IMP-8 satellites. The
72 wavelet transform, particularly continuous wavelet transforms, which helps to understand the
73 behavior of the energy at different scales and the cross-correlation techniques to find the relation
74 between the relativistic electron and different parameters of the solar wind have been
75 implemented. The detailed explanation of the theory associated can be found in various research
76 papers [eg. Adhikari et al., 2015, 2017(a), 2018; Usoro A. E., 2015].

77

2.1 Continuous Wavelet Transform

78 Wavelet transform is an effective mathematical tool for the analysis of transient signals. A
79 continuous wavelet transform (CWT) maps a one-dimensional signal to a two-dimensional time-
80 scale that produces a time- frequency decomposition of the signal which segregates individual
81 signal components constructively unlike the short time Fourier transforms (STFT). The square
82 modulus of the wavelet coefficient, in analogous to the Fourier analysis, lays out the energy
83 distribution in the time-scale plane [Adhikari et al., 2018]. In our study, using CWT scaleogram,
84 the vertical axis provides the information of periodicity at different scales as a function of time in
85 horizontal axis. It helps to comprehend the behavior and distribution of the energy at different
86 scales [Adhikari et al., 2017b]. The detailed analysis of CWT are shown in Figure 5.

87

2.2 Cross-correlation

88



Cross-correlation is the standard, multi-time scale, statistical tool that helps out to obtain the time-delay, determine the similarities, draw similar relative characters and can furnish with the new information [Adhikari et al., 2018]. The time scale is used to determine the lead or lags between the parameters after establishing their correlation. The horizontal plane includes the time (minutes) ranging different values and vertical plane indicates cross-correlation coefficient [Adhikari et al., 2017a]. The detailed analysis of different events are shown in Figure 6. We have taken four different events as listed in table 1.

Events	Year/Month/day	SYM-Hvalue(nT)	Event type
Event 1	2007/01/25	0 to -50	Quiet period
Event 2	2008/09/04	-50 to ≥ -100	Moderate
Event 3	2006/12/15	-100 to ≥ -250	Intense
Event 4	2001/03/31	≤ -250	Super intense

Table 1: Selected storm events, their occurrence time frame in year, month, and day, SYM-H value (nT), and event types are listed out.

3. Results and Discussion

The relativistic electron population in the outer radiation belt is extremely volatile during periods of enhanced geomagnetic activity. Electron fluxes are commonly seen to be depleted during the storm main phase, fluxes can recover to pre-storm levels in the recovery phase and stay depleted or build up to exceed pre-storm levels [Reeves et al., 2003; Meredith et al., 2011]. The flux dropout can be a combination of adiabatic and non-adiabatic effects and losses through the magnetopause and atmospheric precipitation [Millan and Thorne, 2007]. In this work, we have selected four different events depicted in Table 1. The selection of storm types is based on the SYM-H value in accordance with the explanation by Perreault et al., [1978]; Gonzalez et al., [1994]; and Wanliss et al., [2006].

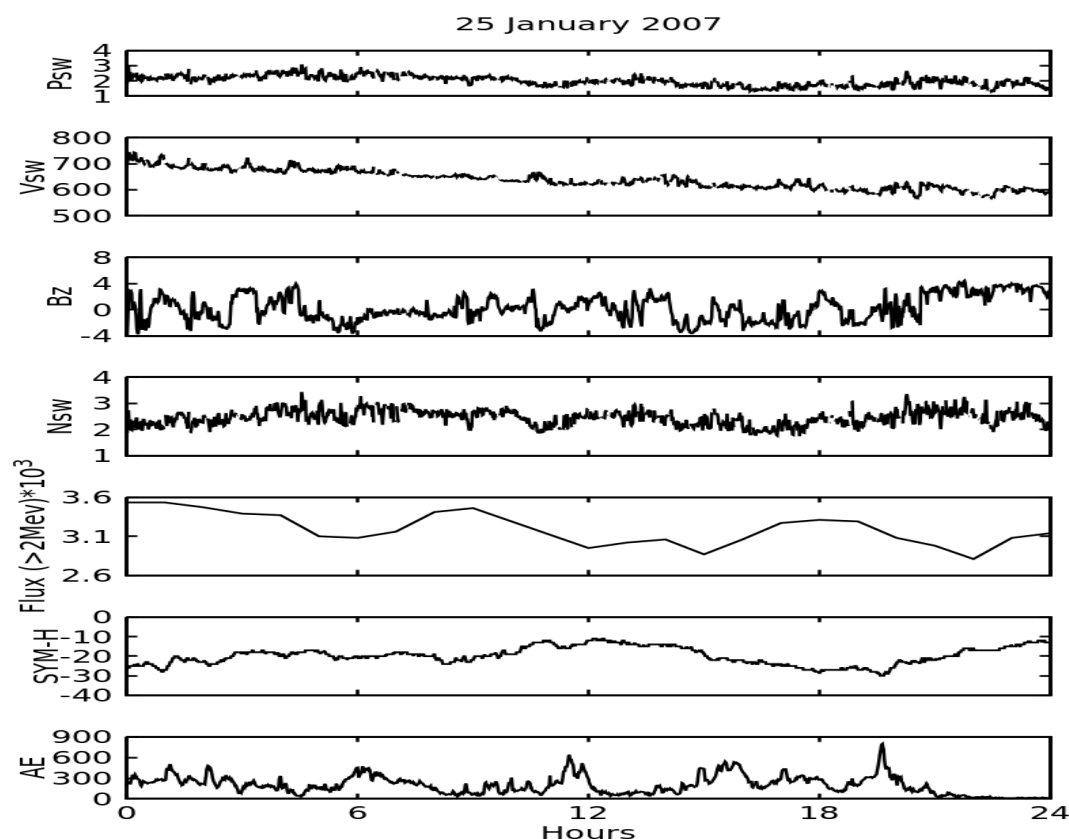
3.1.1 Event 1: The Quietest day (January 25, 2007)



Figure 1 depicts the quietest day, 25th January 2007. The value of SYM-H, on sixth panel, falls to minimum of -30 nT at ~20:00 UT and at the same time IMF-Bz~-4. In fact, the fluctuation of IMF-Bz is mostly southward for almost the entire day with small variations, may be due to the presence of Alfvén waves [Adhikari et al., 2015]. The first panel at the top of the Figure 1 represents the fluctuation of solar wind pressure (~2 nPa to ~2.5 nPa). The second panel shows the fluctuation of solar wind (V_{sw}) (~750 km/s at 00:00 UT and gradually decreases to its lowest value of ~600 km/s towards the end of the day). The fluctuation of solar plasma density (N_{sw}) is represented by fourth panel (value lies between ~2 to ~3 n/cc). As the solar wind pressure is not so high enough to compress the magnetosphere, the high speed solar wind will bring the energetic solar wind plasma into the magnetosphere. Since, the IMF-Bz component is mostly southward through the day with little fluctuation, allowing the energetic particles to inject into the magnetosphere. Thus, the relativistic electron fluxes ($E > 2$ MeV) seems to be populated in the radiation belt showing maximum value of $\sim 3500 \text{ cm}^{-2} \text{ s}^{-1} \text{ sr}^{-1}$, here after we call flux unit as 'FU' for convenience, with slight fluctuation recording its lowest value of ~2700 FU at 22:00 UT (shown in the fifth panel of Figure 1). As high speed solar wind streams come in contact with the magnetosphere, the electrons gain their acceleration [Baker et al., 1993; Paulikas et al., 1978]. The bottom panel indicates the fluctuation of AE index, reaching maximum of ~800 nT corresponding to the minimum value of SYM-H.

135

136



137

138 **Figure 1:** From top to bottom, the panels show the variations of: solar wind pressure (Psw in
 139 nPa), solar wind speed (Vsw in km/s), interplanetary magnetic field (Bz in nT), solar wind
 140 plasma density(Nsw in n/cc), relativistic electron flux $E > 2 \text{ MeV}$ (Flux in $\text{cm}^{-2}\text{S}^{-1}\text{Sr}^{-1}$),
 141 symmetric horizontal component of magnetic field (SYM-H in nT), and auroral electrojet (AE in
 142 nT) indices with time (Hours) respectively for event-1 of 25 January 2007.

143

144 3.1.2 Event 2: Moderate Storm (September 04, 2008)

145 Figure 2 shows the fluctuations in different interplanetary structures during a moderate storm
 146 occurred on September 04, 2008. The sequence of panel is same as that explained in previous
 147 event. The value of SYM-H drops down to $\sim 70 \text{ nT}$ indicating the storm as moderate storm as
 148 defined by [Perreault et al., 1978; Wanliss et al., 2006]. The fluctuation of IMF Bz(in third
 149 panel), directed southward during storm main phase, allowing the charge particles to enter easily
 150 in the magnetosphere[Lemaire, J. F.,2012].The seventh panel shows the fluctuation of AE index



151 with value ~ 1600 nT corresponding to lowest value of IMF-Bz, indicating the normal auroral
152 activities. The first panel at the top of figure 2 shows the solar wind pressure around ~ 9 nPa at the
153 early phase of the storm at 01:00 UT and gradually goes on decreasing to attain a lowest value
154 of ~ 1 nPa at the end of the day. The fluctuation of solar wind velocity at the second panel shows
155 the gradual increment of its magnitude which is about 480 km/s at 00:00 UT and reaching 600
156 km/s at 19:00 UT. The flux of relativistic electron is almost constant with value ~ 100 FU
157 until 16:00 UT and then starts to accelerate to maximum value of ~ 2900 FU at 24:00 UT.
158 Rothwell and McIlwain [1960] formulated a general pattern of the relativistic electron dynamics
159 during a geomagnetic storm. On the study of 276 geomagnetic storms, Reeves et al. [2003] found
160 that only 53% were associated with an enhancement event at geostationary orbit, while 19%
161 were associated with a net flux loss, and 28% showed no significant change which are in
162 agreement with other studies [e.g., Moya et al., 2017; Turner et al., 2013; Zhao & Li, 2013],
163 confirming that solar storms are not always associated with enhancement or depletion in
164 relativistic electron fluxes. Moreover, Wladislaw Lyatsky and Khazanov [2008] found that both
165 V_{sw} and N_{sw} provide a strong effect on relativistic electrons. Furthermore, Reeves et al., [2011]
166 have shown that relativistic electron enhancements are correlated (however, not linearly) with
167 the presence of high-speed solar wind streams and southward IMF during the recovery phase of a
168 geomagnetic storms. Higher the solar wind velocity, higher would be the probability of energetic
169 electron buildup after a storm activity (the recovery phase); during which the evolution of sub
170 storm activity may be due to the gradual enhancement of relativistic electron [Kilpua et
171 al., 2015]. Anderson et al. [2015] showed that the impact of acceleration and loss of relativistic
172 electrons on radiation belt seems to be negligible in comparison to both small and large
173 geomagnetic storms.

174

175

176

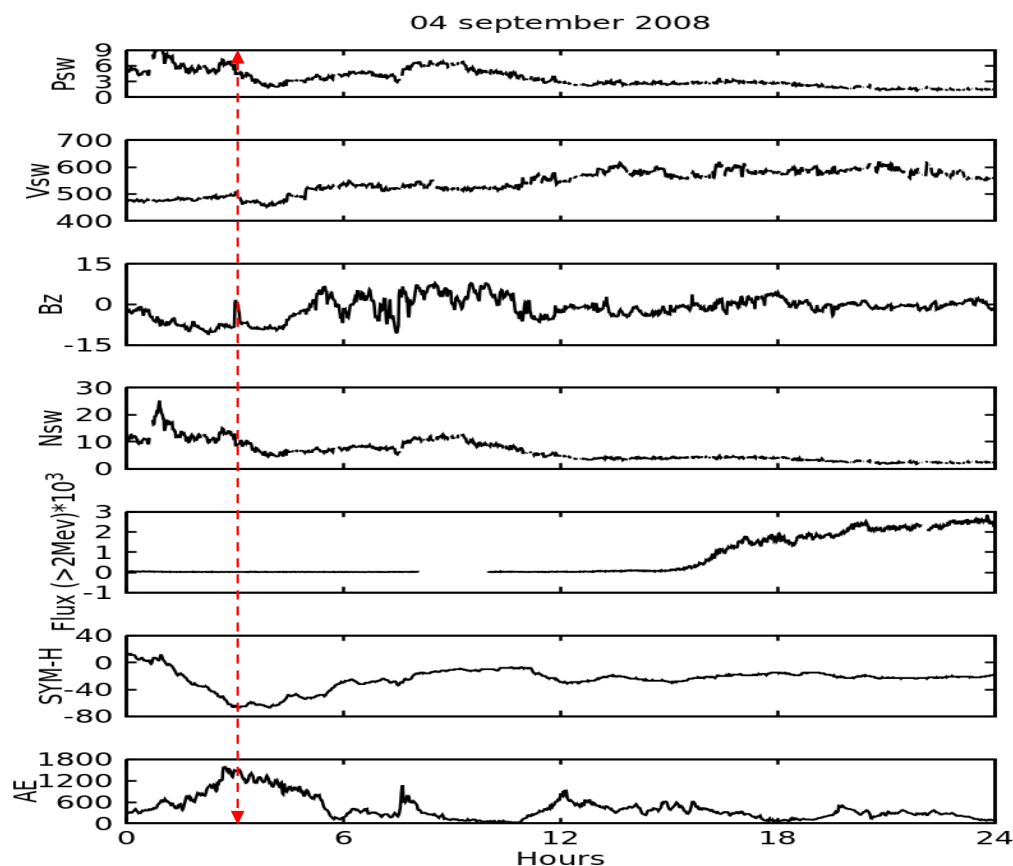


Figure 2: From top to bottom, the panels show the variations of: solar wind pressure (Psw in nPa), solar wind speed (Vsw in km/s), interplanetary magnetic field (Bz in nT), solar wind plasma density (Nsw in n/cc), relativistic electron flux $E > 2 \text{ MeV}$ (Flux in $\text{cm}^{-2}\text{S}^{-1}\text{Sr}^{-1}$), symmetric horizontal component of magnetic field (SYM-H in nT), and auroral electrojet (AE in nT) indices with time (Hours) respectively for event-2 of 04 September, 2008.

3.1.3 Event 3: The Intense Geomagnetic storm (December 15, 2006)

Figure 3 shows the fluctuation of solar wind parameters, component of interplanetary magnetic field Bz, flux of relativistic electrons ($E > 2 \text{ MeV}$) geomagnetic indices SYM-H, and AE during an event on December 15, 2006. The fluctuation pattern of these parameters is as same as that defined in previous events. In the fifth panel of Figure 3, SYM-H shows maximum disturbance of about $\sim -220 \text{ nT}$ at 01:00 UT and stays under -100 nT until 12:00 UT, indicating the storm



185 condition as intense geomagnetic storm as categorized by [Perreault et al., 1978; Wanliss et al.,
186 2006]. In the last (seventh) panel the fluctuation of AE index is shown which reaching its value of
187 around ~1200 nT corresponding to which the IMF Bz (shown in third panel) shows ~-18nT
188 continuing to recover towards northern direction. In the fifth panel, we have the fluctuation of
189 relativistic electron flux which is almost constant during the storm time attaining the value of
190 about ~1100 FU until 12:00 UT and abruptly accelerating to maximum of ~46000 FU at 14:00
191 UT for almost an hour and steeping towards normal. The high solar wind speed (reaching the
192 value of ~850 km/s at 01:00 UT, as shown in second panel) meant the injection of larger amount
193 of relativistic electron flux inside the radiation belt. Instead, the fluxes were seen to be depleted
194 and rather increasing its value for few hours as the velocity decreases to ~600km/s during the
195 recovery phase. Reeves et al., [2003] analyzed the data set that compared 15 years of solar wind
196 data of MeV electrons flux, resulting the high solar wind speeds not as the primary factor for
197 enhancement of relativistic electrons; instead, increment in southward IMF value is the essential
198 condition to cause acceleration of MeV electrons in the outer radiation belt. In addition,
199 Borovsky and Denton, [2005] found that for high-speed stream-driven storms, there is
200 considerable spatial overlap of the super-dense ion plasma sheet with plasmaspheric drainage
201 plumes. This would lead to growth of electromagnetic ion-cyclotron waves that can cause
202 relativistic electron precipitation loss. Since the super dense plasma sheet is associated with high
203 Nsw, large Nsw would enhance such loss. This seems to be the case for this event as well. The
204 first panel shows the fluctuation of solar pressure which remains under 4 nPa throughout the
205 event.

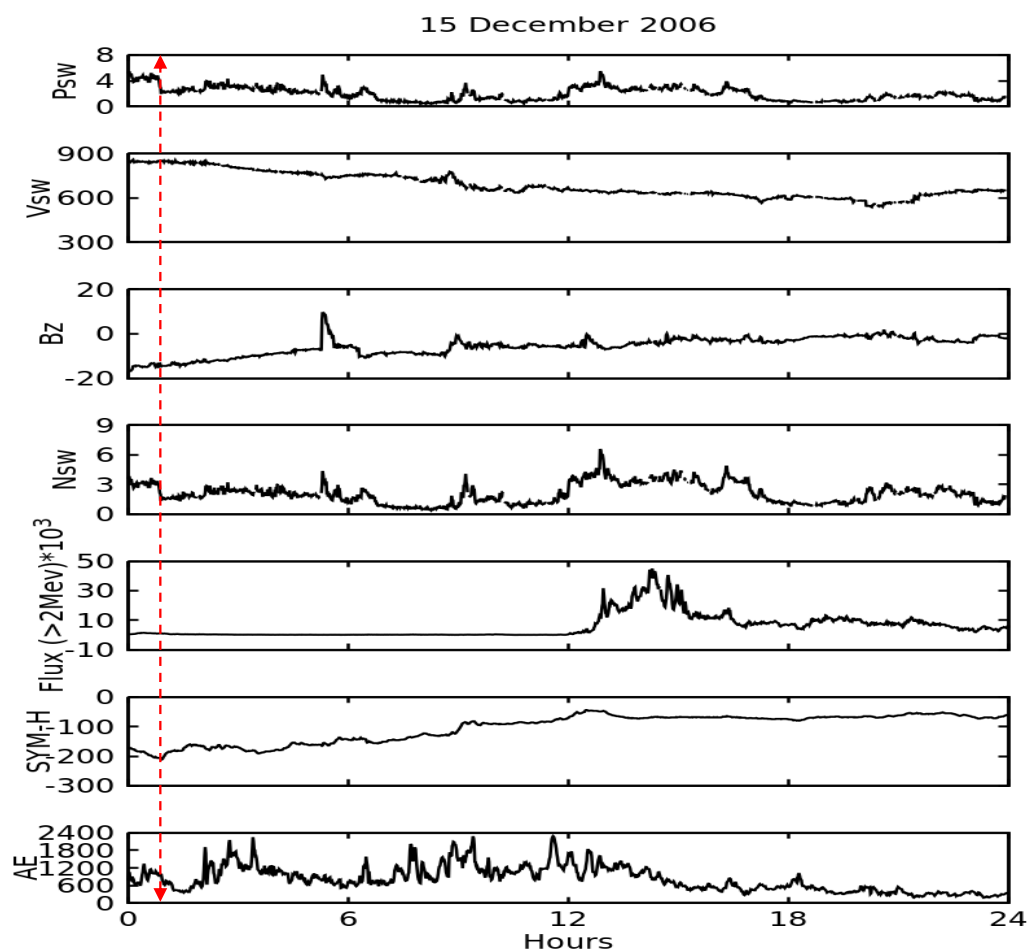


Figure 3: From top to bottom, the panels show the variations of: solar wind pressure (Psw in nPa), solar wind speed (Vsw in km/s), interplanetary magnetic field (Bz in nT), solar wind plasma density (Nsw in n/cc), relativistic electron flux $E > 2 \text{ MeV}$ (Flux in $\text{cm}^{-2} \text{ s}^{-1} \text{ sr}^{-1}$), symmetric horizontal component of magnetic field (SYM-H in nT), and auroral electrojet (AE in nT) indices with time (Hours) respectively for event-3 of 15 December 2006.

3.1.4 Event 4: The super intense storm (March 31, 2001)

In the figure 4, the panels from top to bottom, show solar wind pressure (Psw), solar wind velocity (Vsw), Southward component of magnetic field (IMF-Bz), the solar wind density (Nsw), relativistic electron flux ($E > 2 \text{ MeV}$), the geomagnetic indices SYM-H, and AE during



212 march 31, 2001 respectively. In addition, in the sixth panel, the gradual decay of SYM-H value
 213 up to -410 nT at around 08:00 UT indicates the occurrence of geomagnetic storm as super-
 214 intense [Perreault et al., 1978; Wanliss et al., 2006]. The rapid fluctuation of solar wind
 215 parameters started with the compression of bow shock at around 01:00 UT. The main event
 216 occurred at around 08:00 UT and lasted for several hours. The third panel shows the variation of
 217 IMF-Bz component, having strongly negative value ~ -50 nT at 06:00 UT until 08:00 UT
 218 corresponding to the SYM-H value of ~ -410 nT indicating that the magnetopause was briefly
 219 pushed inward of geostationary orbit, IMF Bz turned very dynamic, fluctuating between ~ -50 nT
 220 and $\sim +50$ nT, allowing the charged particles to penetrate repeatedly into the magnetosphere
 221 causing high auroral activity (AE ~ 2400 nT, shown in seventh panel). During the initial phase of
 222 main storm, the solar wind velocity shows abrupt increment upto ~ 850 km/s which then
 223 maintains to ~ 700 km/s during storm main phase. At the same time, the solar wind pressure (first
 224 panel of figure 4) elevates to maximum value of ~ 60 nPa at the initial phase of the storm and then
 225 decreases to ~ 20 nPa at 06:00 UT, maintaining same throughout the day. The fluctuation of Nsw
 226 with maximum peak value about ~ 60 n/cc at 05:00 UT, as shown in fourth panel of figure 4,
 227 followed by the decreases in its value and thereafter low fluctuation is observed. The flux of
 228 relativistic electron, shows maximum value of ~ 740 FU at 00:00 UT and decreases to ~ 160 FU
 229 after 01:00 UT. The possible mechanism for this scenario is that for high-speed stream driven
 230 storms, there is a considerable spatial overlap of super dense ion plasma sheet with
 231 plasmaspheric drainage plumes [Borovsky and Denton, 2009]. This would lead to the growth of
 232 electromagnetic ion-cyclotron waves that can cause relativistic electron precipitation loss. As the
 233 super dense plasma sheet is associated with high Nsw, large Nsw would enhance such loss [Li et
 234 al., 2011]. This implies that Nsw clearly plays a crucial role in relativistic electron loss.
 235 However, the strong effect of solar wind density on relativistic electron is relatively unexpected
 236 because the former is not a primary factor in the generation of geomagnetic disturbance [Wanliss
 237 and Showalter, 2006]. Nevertheless, the possible effects of solar wind density on relativistic
 238 electron may be due to the compression of dayside magnetosphere, by high-density solar wind,
 239 acting as shielding in the inner atmosphere thus preventing the penetration of the large-scale
 240 electric fields ultimately leading to losses of relativistic electron from the outer radiation belt.
 241 This indicates the implicit effect of Nsw on relativistic electron.

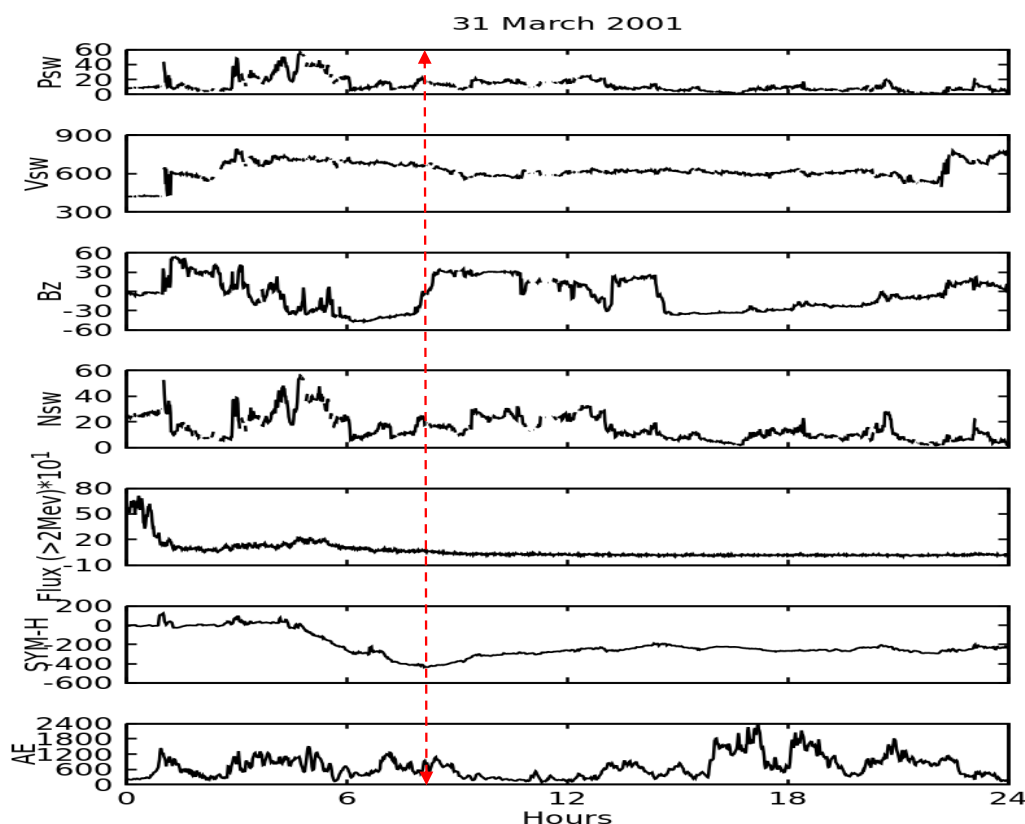


Figure 4: From top to bottom, the panels show the variations of: solar wind pressure(Psw in nPa), solar wind speed (Vsw in km/s), interplanetary magnetic field (Bz in nT), solar wind plasma density(Nsw in n/cc), relativistic electron flux $E > 2 \text{ MeV}$ (Flux in $\text{cm}^{-2}\text{S}^{-1}\text{Sr}^{-1}$), symmetric horizontal component of magnetic field (SYM-H in nT), and auroral electrojet (AE in nT) indices with time (Hours) respectively for event-4 of 31 March 2001.

3.2 Continuous Wavelet Transform

Figure 5 depicts the scalograms for the relativistic electrons ($E > 2 \text{ MeV}$). In Figure 5, magenta indicates the highest power areas while red represents low power areas value as shown on the vertical color bar of each plot on the right. Furthermore, Time (in minutes) are placed on the horizontal axis whereas period (in minutes) in the vertical axis.

Figure 5 (a) represents the scalogram for the main event of intense storm, stronger wavelet power areas of flux intensities between 0.4-0.7 FU are accumulated around 65-85 minutes at the time



scales (period) range of 14-16 minutes. This shows the flow of energy lasted for few minutes, the low flux intensities (less intense power area) dominated the event. Figure 5 (b) and (c) represents the scalogram plot for the main event of super-intense and moderate storm respectively. Moreover, the wavelet powers areas of higher flux intensities ranging from 1.2 to 2 FU are found to be distributed at lower to higher time scales range of 2-15 minutes throughout the event time. In Figure 5(b), the highest power areas is around 60-100 minutes at time scales approximately 1-3 minutes and again at time scales approximately 10-15 minutes. The other power areas covered by blue color are seen scattered at different times throughout the time scales between 10-170 minutes. Figure 5(c) shows the scalograms for moderate storm where the highest power area is around 65-85 minutes at time scales approximately 14-16 minutes. The other power areas covered by blue color are seen around 60-90 minutes at timescales between 12-16 minutes. Furthermore, such variation of flux intensities on both figures resemble the highly perturbed state during the happening of main event as compared to the quiet event shown in Figure 5 (d), where low intensities dominated the wavelet powers areas at different times and scales. The power areas covered by green color are seen distributed discontinuously over the cone of influence. The non-uniform distribution of energy at different time scales inconsistent with time strongly suggests the true dynamic nature of relativistic electron flux. This observation insists that the geomagnetic storm is not the primary cause of accumulation or loss of charge particles over the radiation belt. In fact, it shows event-specific behavior.

270

271

272

273

274

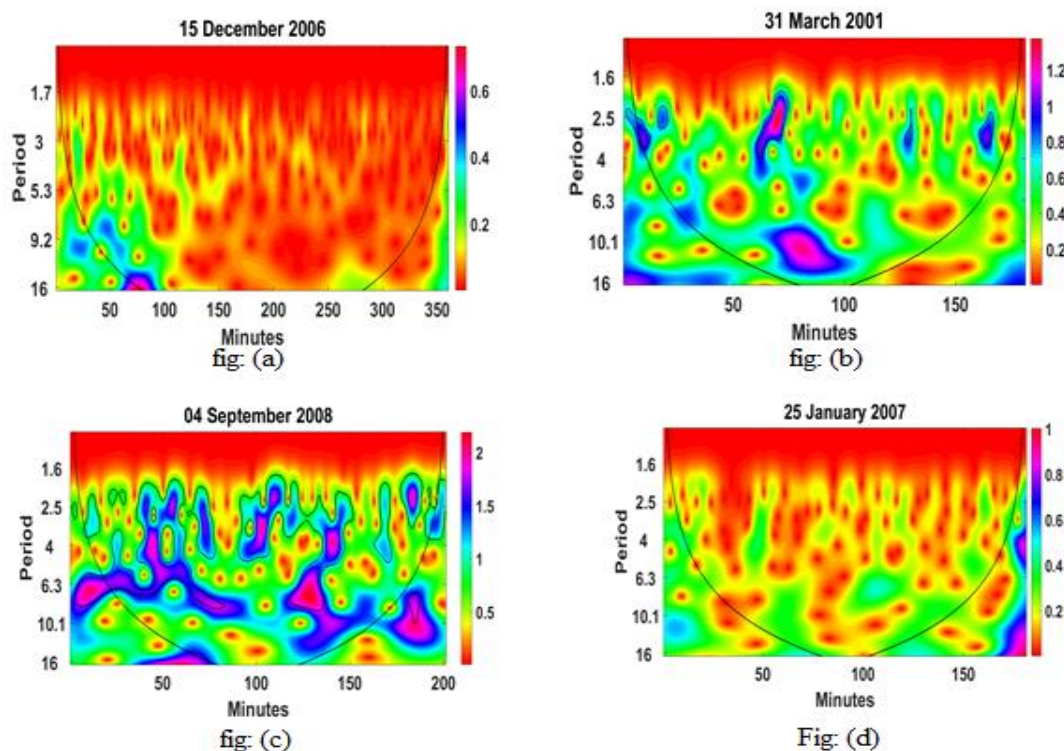


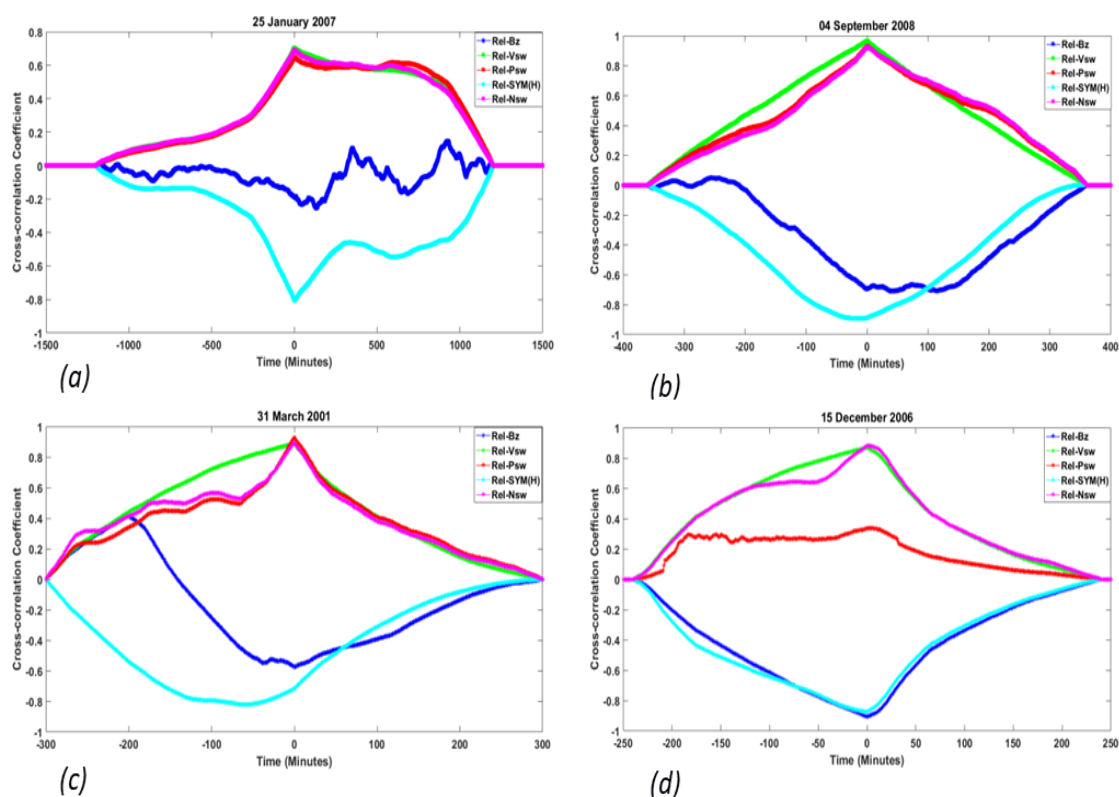
Figure 5: Scalograms for the relativistic electron flux (Rel.) $E > 2 \text{ MeV}$ for (a) Intense storm, 15 December, 2006 (b) Super intense storm, 31 March, 2001 (c) Moderate storm, 04 September, 2008, and (d) Quiet Period, 25 January, 2007.

3.3 Cross Correlation

Figure 6 shows the cross-correlation between the relativistic electron flux $E > 2 \text{ MeV}$ (Refer to as Rel. in legend) with different solar parameters. It is clearly evident that the magenta curve (Rel.-Nsw), green curve (Rel.-Vsw) and red curve (Rel.-Psw) almost overlap to each other and attains a good positive correlation with cross-correlation coefficient of 0.9 at lags of 0 minute (when no lags is applied). In addition, no large variation is observed in the value of cross-correlation coefficient for relativistic electron flux and solar wind velocity during main phase of three geomagnetic storm events (our work) and a geoeffectively quiet event. This suggests that high solar wind velocity is an important condition for enhancing the high radiation belt electron fluxes but not a determining condition. However, on intense storm, fig (d), the red curve shows weak correlation with cross-correlation coefficient of 0.3. Indeed, this result is expected as Vsw,



290 Psw, and Nsw are taken as the plausible factors for the fluctuation of relativistic electron in outer
 291 radiation belt [Wladislaw Lyatsky and Khazanov, 2008]. Li et al. [2005] studied the cross-
 292 correlation of electron flux at 50 Kev to 2 MeV energies with Vsw; the strong correlation with
 293 zero lag for low energies and longer lags for higher energies was observed. Paulikas and Blake
 294 [1979, 2010] found a good correlation between the solar wind velocity and the MeV electron
 295 flux at geostationary orbit. However, they found out the unprecedented complex relationship
 296 between solar wind velocity and radiation belt electron fluxes. It has also been established that
 297 high-speed solar wind and geomagnetic activity are strongly associated with the appearances of
 298 relativistic electrons [Baker et al., 1993]. For the identification of relativistic electrons, the rapid
 299 increment of the sustained solar wind velocity greater than 450 km/s acts as a strong external
 300 indicator [Reeves et al., 2001]. In each of the events, SYM-H seems to be negatively
 301 correlated (in fact it is about 85-90% in average) and so does the IMF Bz. Hence it is not a
 302 reliable predictor as decrease in SYM-H value is not necessarily for relativistic event to occur.
 303



304



Figure 6: Cross correlation between Relativistic electron flux ($E > 2\text{MeV}$) with Bz (blue), Vsw (green), Psw (red), SYM-H (sky blue) and Nsw (pink) during (a) Quiet Period, 25 January, 2007 (b) Moderate storm, 04 September, 2008 (c) Super intense storm, 31 March, 2001 and (d) Intense storm, 15 December, 2006 .

305

306 4. Conclusion

307 In this paper, we have analyzed various solar wind parameters and geomagnetic indices with
 308 relativistic electron flux ($E > 2\text{MeV}$) datasets for the four geomagnetic events selected. To
 309 enhance the analysis of relativistic electron flux, the cross-correlation and CWT analysis was
 310 adopted [Adhikari 2015; Adhikari et al. 2017a, b; Adhikari et al., 2018]. The work presented
 311 here shows good correlation, having positive cross-correlation coefficient (> 0.8), for
 312 relativistic electron flux with the solar wind velocity, pressure, and solar density. Thus, the
 313 choosing of these parameters are well justified as they are highly geoeffective. In each of the
 314 event, except super-intense, whenever the solar wind exceeds 600 km/s, there seems to increase
 315 in relativistic electron flux. This is consistent with previous results which shows a large average
 316 solar wind speed ($V_{sw} > 500\text{ km/s}$) is characteristic of enhancement events [Paulikas & Blake
 317 1978, 2010; Reeves et al., 2011].

318 As depicted in the event-4 (Figure 4), with the increase in solar wind dynamic pressure, the
 319 electron flux shows a decrement factor of 3. The solar wind dynamic pressure and IMF Bz play
 320 indispensable role in causing the relativistic flux dropouts as the magnetopause is compressed
 321 closer to earth or located very far ($> 10\text{ Earth Radii}$) [Gao et al., 2015]. The impingement of high
 322 speed solar wind, suppressing the dayside magnetosphere enhancing the drift shell splitting of
 323 charged particles, has impacts on the possible loss mechanisms of the magnetospheric relativistic
 324 electron, as in the case of super intense storms (super sub-storms). Our result substantiates the
 325 geomagnetic storms are not a primary factor that pumps up the radiation belt. In fact, the
 326 geomagnetic storms can deplete, enhance or cause little effect on the outer radiation belt. To be
 327 precise, it shows event-specific behavior.

328 In addition, all the geomagnetic storm events, except intense storm, Psw is found to be highly
 329 and positively correlated with relativistic electron flux. The higher Psw leads to the depletion of
 330 the electron flux presumably through compressing the inner magnetosphere and intensifying the



331 ring current [Gao et al., 2015]. However, for intense storm, Psw is found to be weakly correlated
 332 followed by an abrupt increase of electron flux value for ~4 hrs, which is interesting and unique.

333

334 In sum, the count of relativistic electron flux (> 2 MeV) decreases during the main phase of
 335 geomagnetic storm with the increase in -- from quiet to super intense storm -- geomagnetic storm
 336 conditions (Table 1). Furthermore, in case of intense geomagnetic storm: during the post-storm
 337 condition, sharp increase in flux count (even larger than in normal quiet condition) is observed,
 338 inkling of unperturbed ionosphere which might be the precursor for any sort of space weather
 339 effects in near future. Thus, there is a need of careful and extensive study of large events over
 340 extended period through more advanced tools and techniques for better understanding of the
 341 inherent physical mechanism.

342

343 **Acknowledgements:**

344 The solar wind, interplanetary magnetic field, geomagnetic indices and relativistic electrons data
 345 for this study were obtained from <https://omniweb.gsfc.nasa.gov/>. T.Thapa acknowledges the
 346 grant for M.Sc dissertation from the B.P.Koirala Memorial Planetarium.

347

348

349 **Conflict of interest statement**

350 On behalf of all authors, the corresponding author states that there is no conflict of interest.

351 **Financial and Ethical disclosures-**

352 No Funding. Request to waive publication fees.

353

354 **Authors should include the following statements (if applicable) in a separate section**
 355 **entitled "Compliance with Ethical Standards" when submitting a paper**

356 Disclosure of potential conflicts of interest research involving human participants and/or animals
 357 informed consent.

358

359

360

361



362 References

- 363 Adhikari, B., and N. P. Chapagain (2015), Polar cap potential and merging electric field
 364 during high intensity long duration continuous auroral activity, *J. Nepal Phys. Soc.*, **3(1)**,
 365 37.
 366
 367 Adhikari, B, P. Baruwat, and N. P. Chapagain (2017a), Analysis of supersubstorm events
 368 with reference to polar cap potential and polar cap index, *Earth Space Sci.*, **4(1)**, 2-15.
 369
 370 Adhikari, B, R. Adhikari, N. P. Chapagain, N. Sapkota, S. Dahal, D. Pandit (2017b),
 371 Daily, Seasonal and Monthly Variation of Middle-low latitudes Magnetic Field during
 372 Low Solar Activity. *Discovery*, **53(255)**, 31, 34, 35, 36.
 373
 374 Adhikari, B., Dahal, S., Sapkota, N., Baruwat, P., Bhattarai, B., Khanal, K., & Chapagain,
 375 N. P. (2018), Field-aligned and polar cap potential and geomagnetic disturbances: A
 376 review of cross-correlation analysis, *Earth Space Sci.*, **5**, [https://doi.](https://doi.org/10.1029/2018EA000392)
 377 [org/10.1029/2018EA000392](https://doi.org/10.1029/2018EA000392),
 378
 379 Anderson, B. R., R. M. Millan, G. D. Reeves, and R. H. W. Friedel (2015), Acceleration
 380 and loss of relativistic electrons during small geomagnetic storms, *Geophys. Res. Lett.*,
 381 **42**, 10,113–10,119, doi: 10.1002/2015GL066376.
 382
 383 Baker, D. N., G. M. Mason, O. Figueroa, G. Colon, J. G. Watzin, and R. M. Aleman
 384 (1993), An overview of the solar, anomalous, and magnetospheric particle explorer
 385 (SAMPEX) mission, *IEEE Trans, Geosci. Rem. Sensing*, **31(3)**, 4, 39.
 386
 387 Baker, D. N. (2000). The occurrence of operational anomalies in spacecraft and their
 388 relationship to space weather, *IEEE Transactions on Plasma Science*, **28(6)**, 2007–2016.
 389
 390 Borovsky, J. E., and M. H. Denton, (2005), Differences between CME-driven storms and
 391 CIR-driven storms, *J. Geophys. Res.*, **111**, A07S08, doi: 10.1029/2005JA011447.
 392
 393 Elkington, S. R., Hudson, M. K., & Chan, A. A., (1999), Acceleration of relativistic
 394 electrons via drift-resonant interaction with toroidal-mode PC-5 ULF oscillations.
 395 *Geophys. Res. Lett.*, **26**, 3273–3276.
 396
 397 Gao, X., Li, W., Bortnik, J., Thorne, R. M., Lu, Q., Ma, Q. Wang, S. (2015), The effect of
 398 different solar wind parameters upon significant relativistic electron flux dropouts in the
 399 magnetosphere. *J. Geophys. Res. Space Physics*, **120**, 4324–4337.
 400 <https://doi.org/10.1002/2015JA021182>
 401
 402 G.D. Reeves, R. Friedel, T. P. O'Brien, R. L. McPherron, D. Sornette and H. J. Singer
 403 (2001), Which magnetic Storms Produce relativistic electrons at geosynchronous orbit? *J.*
 404 *Geophys. Res.*, **106**, N0. A8, 49.
 405



- 406 Gonzalez, W.D., Joselyn, J.A., Kamide, Y., Kroehl, H.W., Rostoker, V., Tsurutani, B.T.
 407 and Vasyliunas, V.M., (1994), What is a geomagnetic storm, *J. Geophys. Res.*, **99**:5771.
 408
- 409 Gosling, J.T., Mccomas, D.J., Philips, J.L and Bame, S.J., (1991), Geomagnetic activity
 410 associated with earth passage of interplanetary shock disturbances and coronal mass
 411 ejections, *J. Geophys. Res.*, **96**: 7831.
 412
- 413 Kilpua, E. K. J., Hietala, H., Turner, D. L., Koskinen, H. E. J., Pulkkinen, T. I.,
 414 Rodriguez, J. V., Reeves, G. D., Claudepierre, S. G., and Spence, H. E. (2015),
 415 Unraveling the drivers of the storm time radiation belt response: RADIATION BELT
 416 AND STORM DRIVERS, *Geophys. Res. Lett.*, **42**, 3076–3084,
 417 doi:10.1002/2015GL063542.
 418
- 419 Lemaire, J. F. (2012), The effect of a southward interplanetary magnetic field on
 420 Stormer's allowed regions, *Adv. Space Res.*, **V-31(5)**.
- 428 Li, X., D. N. Baker, M. Temerin, G. Reeves, R. Friedel, and C. Shen (2005), Energetic
 429 electrons, 50 keV to 6 MeV, at geosynchronous orbit: Their responses to solar wind
 430 variations, *Space Weather*, **3**, S04001, doi:10.1029/2004SW000105
 431
- 432 Li, X., M. Temerin, D. N. Baker, and G. D. Reeves (2011), Behavior of MeV electrons at
 433 geosynchronous orbit during last two solar cycles, *J. Geophys. Res.*, **116**, A11207,
 434 doi:10.1029/2011JA016934, 43.
 435
- 436 Mauk, B. H., N. J. Fox, S. G. Kanekal, R. L. Kessel, D. G. Sibeck, and A. Ukhorskiy
 437 (2012), Science objectives and rationale for the radiation belt storm probes mission,
 438 *Space Sci. Rev.*, **179**, 3–27, doi:10.1007/s11214-012-9908-y.
 439
- 440 Meredith, N. P., Horne, R. B., Lam, M. M., Denton, M. H., Borovsky, J. E., & Green, J.
 441 C. (2011), Energetic electron precipitation during high-speed solar wind stream driven
 442 storms., *J. Geophys. Res.*, **116**, A05223. https://doi.org/10.1029/2010JA016293
 443
- 444 Millan, R. M. and Thorne, R. M. (2007), Review of radiation belt relativistic electron
 445 losses, *J. Atmos. Sol. Terr. Phys.*, **69**, 362–377, doi:10.1016/j.jastp.2006.06.019.
 446
- 447 Miyoshi, Y., Morioka, A., Misawa, H., Obara, T., Nagai T., and Kasahara, Y., (2003),
 448 Rebuilding process of the outer radiation belt during the 3 November 1993 magnetic
 449 storm: NOAA and Exos-D observations, *J. Geophys. Res.*, **108**, 1004,
 450 doi:10.1029/2001JA007542.
 451
- 452 Morley, S., Friedel, R., Henderson, M., Cayton, T., Cunningham, G., Blake, J.,
 453 Christensen, R., and Thomsen, D., (2011). On the relationship between relativistic
 454 electron flux and solar wind velocity: Paulikas and Blake revisited. *J. Geophys. Res.*, **116**,
 455 10.1029/2010JA015735.
 456



- 457 Moya, P. S., Pinto, V. A., Sibeck, D. G., Kanekal, S. G., and Baker, D. N. (2017), On the
 458 effect of geomagnetic storms on relativistic electrons in the outer radiation belt: Van
 459 Allen Probes observations. *J. Geophys. Res.*, **122**, <https://doi.org/10.1002/2017JA024735>.
 460
- 461 Murphy, K. R., Watt, C. E. J., Mann, I. R., Jonathan Rae, I., Sibeck, D. G., Boyd, A. J., et
 462 al. (2017), The global statistical response of the outer radiation belt during geomagnetic
 463 storms, *Geophys. Res. Lett.*, **45**, doi: 10.1002/2017GL076674.
 464
- 465 Paulikas, G. A. and Blake, J. B. (1978), Effects of the solar wind on magnetospheric
 466 dynamics: Energetic electrons at the synchronous orbit, *Wiley Online Library*, 18, 19, 39,
 467 49.
 468
- 469 Paulikas, G., and Blake, J. (1979). Effects of the solar wind on magnetospheric dynamics:
 470 Energetic electrons at the synchronous orbit. In W. P. Olson (Ed.), *Geophysical*
 471 *Monograph Series* (pp. 180–202). Washington, DC: *American Geophysical Union*,
 472 [doi:10.1029/GM021p0180](https://doi.org/10.1029/GM021p0180)
 473
- 474 Perreault, P., and Akasofu, S.-I. (1978), A study of geomagnetic storms, *Geophys. J. R.*
 475 *astr. Soc.*, **54**, 3, doi:10.1111/j.1365-246x.1978.tb-05494.x
 476
- 477 Rajkumar Hajra, Bruce T. Tsurutani, Ezequiel Echer, Walter D. Gonzalez, and
 478 Ondrej Santolik (2015), Relativistic ($E > 0.6$, > 2.0 , and > 4.0 MeV) Electron Acceleration
 479 at Geosynchronous orbit during HIGH-INTENSITY, LONG-DURATION,
 480 CONTINUOUS AE ACTIVITY (HILDCAA) events, *The Astrophysical Journal*, 799:39
 481 (8pp), doi:10.1088/0004-637X/799/1/39
- 482 Reeves, E. G. D., K. L. McAdams, R. H. W. Friedel, and T. P. O'Brien (2003),
 483 Acceleration and loss of relativistic electrons during geomagnetic storms, *Geophys. Res.*
 484 *Lett.*, **30**(10), 1529, doi:10.1029/2002GL016513.
 485
- 486 Reeves, G. D., Morley, S. K., Friedel, R. H. W., Henderson, M. G., Cayton, T. E.,
 487 Cunningham, G., ... Thomsen, D. (2011). On the relationship between relativistic electron
 488 flux and solar wind velocity: Paulikas and Blake revisited, (2010), *J. Geophys. Res.*, **116**,
 489 A02213. <https://doi.org/10.1029/2010JA015735>.
 490
- 491
- 492 Rothwell, P., and C. McIlwain (1960), Magnetic storms and the Van Allen radiation belts
 493 – observations from satellite 1958□ (Explorer IV), *J. Geophys. Res.*, **65**, 52.
 494
- 495 R. Kataoka and Y. Miyoshi (2008), Average profiles of the solar wind and outer
 496 radiation belt, *Ann. Geophys.*, **26**, 1335–1339,
 497
- 498 Schiller, Q., X. Li, L. Blum, W. Tu, D. L. Turner, and J. B. Blake (2014), A nonstorm
 499 time enhancement of relativistic electrons in the outer radiation belt, *Geophys. Res. Lett.*,
 500 **41**, doi:10.1002/2013GL058485, 4,51.
 501



- 502 Tsurutani, B. T., Gonzalez, W. D., Gonzalez, A. L., Guarnieri, F. L., Gopalswamy, N.,
 503 Grande, M., *et al.*, (2006), Corotating solar wind streams and recurrent geomagnetic
 504 activity: A review. *Journal of Geophysical Research: Space Physics*, **111**(A7). DOI:
 505 10.1029/2005ja011273
- 506
 507 Turner, D. L., Shprits, Y., Hartinger, M., & Angelopoulos, V.(2012), Explaining sudden
 508 losses of outer radiation belt electrons during geomagnetic storms. *Nature Physics*, **8**(3),
 509 208–212, <https://doi.org/10.1038/nphys2185>.
- 510
 511 Turner, D.L., V. Angelopoulos, W. Li, M.D. Hartinger, M. Usanova, I.R. Mann, J.
 512 Bortnik and Y. Shprits (2013), On the storm-time evolution of relativistic electron phase
 513 space density in Earth's outer radiation belt, *J. Geophys. Res.*, **118**, 2196–2212,
 514 doi:10.1002/jgra.50151.
- 515
 516 Usoro, A. E. (2015), Some basic properties of cross-correlation functions of n-
 517 dimensional vector time series, *Journal of Statistical and Econometric Methods*, **4**(1), 46.
- 518
 519 Wanliss, J. A. and Showalter, K. M. (2006), High-resolution global storm index: Dst
 520 versus SYM-H, *Journal of Geophysical Research: Space Physics*, **111**(A2), 31, 32.
- 521
 522 Wladislaw Lyatsky and George V. Khazanov (2008.), Effect of solar wind density on
 523 relativistic electrons at geosynchronous orbit. *Geophysical. Res. Letters*, **35**, L03109,
 524 doi:10.1029/2007GL032524, 44, 49.
- 525
 526 Xinliang Gao, Wenli, Jacob Bortnik, Richard M. Thorne, Quanming Lu, Qianli Ma, Xin
 527 Tao and Shui Wang (2015), The effect of different solar wind parameters upon
 528 significant relativistic electron flux dropouts in the magnetosphere, DOI:
 529 10.1002/2015ja021182, *J. of Geophysics*, **120**, 50.
- 530
 531 Zhao, H., & Li, X.(2013). Inward shift of outer radiation belt electrons as a function of
 532 Dst index and the influence of the solar wind on electron injections into the slot region.
 533 *Journal of Geophysical Research: Space Physics*, **118**, 756–764.
 534 <https://doi.org/10.1029/2012JA018179>.
- 535